Variation of the molecular cloud lifecycle across the nearby galaxy population

Jaeyeon Kim[1] , Mélanie Chevance[1,2], J. M. Diederik Kruijssen[2] and Adam K. Leroy[3,4]

[1]Zentrum für Astronomie der Universität Heidelberg, Institut für Theoretische Astrophysik, Albert-Ueberle-Str. 2, 69120 Heidelberg

[2]Cosmic Origins Of Life (COOL) Research DAO, coolresearch.io

[3]Department of Astronomy, The Ohio State University, 140 West 18th Avenue, Columbus, OH 43210, USA

[4]Center for Cosmology and Astroparticle Physics, 191 West Woodruff Avenue, Columbus, OH 43210, USA

Abstract. The processes of star formation and feedback take place on the scales of giant molecular clouds (GMCs; $\sim$100 pc) within galaxies and play a major role in governing galaxy evolution. By applying a robust statistical method to PHANGS observations, we systematically measure the evolutionary timeline from molecular clouds to exposed young stellar regions, across an unprecedented sample of 54 galaxies. These timescales depend on galaxy environment, revealing the role of galactic-scale dynamical processes in the small-scale GMC evolution. Furthermore, in the 5 nearest galaxies of our sample, we have refined the GMC timeline further and established the duration of the heavily obscured phase, using $24\,\mu$m emission. These results represent a major first step towards a comprehensive picture of cloud assembly and feedback, which will be extended to 19 more galaxies with our ongoing JWST Large Program.

Keywords. stars: formation – ISM: clouds – ISM: structure – galaxies: ISM – galaxies: star formation

1. Introduction

Giant molecular clouds (GMCs) are primary sites for star formation. The properties of the clouds are shaped by the large-scale environment of their host galaxies, directly linking the initial conditions of star formation to galactic-scale properties (e.g. Sun et al. 2022). In turn, the energy, momentum and metals deposited by stellar feedback drive the continuous evolution of the interstellar medium (ISM) in general (e.g. Chevance et al. 2022). The characterisation of the evolutionary time-scales from GMC assembly to star formation, and to young stellar regions devoid of cold gas provides important insights into which physical mechanisms regulate this multi-scale cycle, and is therefore crucial to understanding the evolution of galaxies.

Growing evidence from cloud-scale observations is revealing spatial offsets between molecular gas and young stellar regions, and points towards a view of GMCs as transient objects that are dispersed quickly by violent feedback from young massive stars (e.g. Kawamura et al. 2009; Kruijssen et al. 2019; Chevance et al. 2020). This contradicts a conventional view where GMCs are considered to represent quasi-equilibrium structures that survive over a large fraction of a galactic rotation period (e.g. Scoville & Hersh 1979; Koda et al. 2009).

Kruijssen & Longmore (2014) and Kruijssen et al. (2018) developed a statistical method, called the 'uncertainty principle for star formation', which translates the observed spatial decorrelation between gas and young stellar regions into their underlying evolutionary timeline, spanning from cloud assembly to subsequent star formation and cloud dispersal, and finally to young stellar regions free of molecular gas. Applying this method to CO and Hα observations, several works have determined the evolutionary timeline between quiescent molecular gas to exposed young stellar regions for about a dozen of nearby galaxies (Kruijssen et al. 2019; Chevance et al. 2020; Zabel et al. 2020; Kim et al. 2021; Lu et al. 2022; Ward et al. 2022). So far, these time-scale measurements have been limited to a small number of galaxies due to the lack of CO imaging of star-forming discs at cloud-scale resolution and the fact that our method requires us to resolve at least the separation length between independent star-forming regions (100−300 pc). These previous studies did not allow us to identify the key environmental factors and cloud properties (e.g. total, gas, molecular gas surface densities and masses) responsible for setting these time-scales.

In Kim et al. (2022a), we greatly increase the number of galaxies to 54 galaxies, for which the evolutionary sequence between GMCs and young stellar regions has been determined. We capitalise on our CO observations from PHANGS–ALMA (Leroy et al. 2021) and a narrow-band Hα survey by A. Razza et al. (in prep.; PHANGS–Hα). By applying the statistical method described above to these galaxies, we systematically obtain the evolutionary sequence of GMCs from a quiescent molecular cloud phase to a feedback dispersal phase, and finally to a gas-free HII region phase. This statistically representative PHANGS sample covers a large range of galactic properties (∼2 dex in stellar mass) and diverse spiral arm morphologies. This enables us to quantitatively determine the correlations between the small-scale evolutionary cycle of molecular clouds and galactic-scale environmental properties.

2. Evolutionary timeline from molecular gas to young stars in 54 PHANGS galaxies

Here we present the results obtained from the application of our statistical method (Kruijssen & Longmore 2014; Kruijssen et al. 2018) to CO and Hα observations as tracers of molecular gas and star formation rate (SFR) for 54 galaxies in the PHANGS sample. We measure the cloud lifetime ($t_{\rm CO}$), the phase during which both molecular gas and SFR tracers overlap, the feedback time-scale ($t_{\rm fb}$), and the characteristic separation length between independent regions evolving from gas to stars (λ). We also derive the integrated star formation efficiency per cloud lifecycle ($\epsilon_{\rm sf} = t_{\rm CO}\Sigma_{\rm SFR}/\Sigma_{\rm H_2}^{\rm compact}$, where $\Sigma_{\rm SFR}$ and $\Sigma_{\rm H_2}^{\rm compact}$ are the area-weighted average surface densities of SFR and compact molecular gas across the field of view, respectively). In Figure 1, we show the distributions of our main measurements across the galaxy sample.

Across all galaxies in our sample, the range of measured cloud lifetimes is 5−30 Myr, with an average of 16 Myr and a 16−84 percentile range of 11−22 Myr. The range of our measurements of $t_{\rm CO}$ corresponds to 1−3 times the average crossing time-scale of massive GMCs in PHANGS–ALMA (Sun et al. 2022), which suggests that clouds are transient objects that disperse within a small multiple of their dynamical time-scale. For 12 galaxies, we do not sufficiently resolve the separation between independent regions and therefore we are only able to obtain upper limits on $t_{\rm fb}$. Without these galaxies, the range of feedback time-scale becomes 1.3−5.4 Myr, constituting 10−30% of the cloud lifetime, with an average and a standard deviation of 3.2 ± 1.1 Myr. This time-scale represents the time it takes for emerging massive stars (visible in Hα) to disrupt the surrounding molecular gas (either by kinetic dispersal or by the photodissociation of CO molecules).
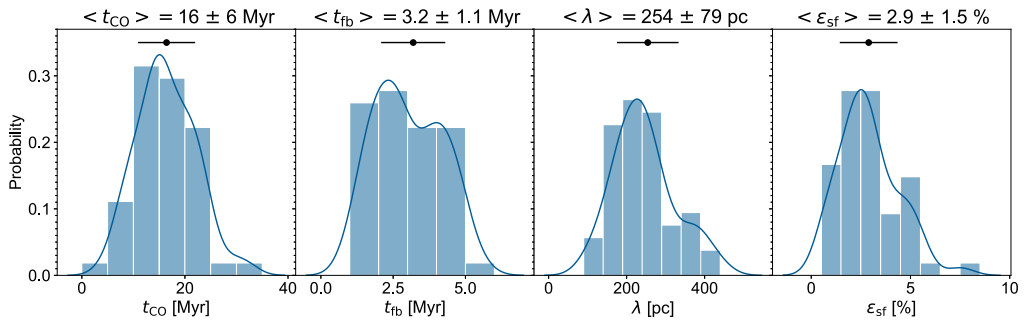
Figure 1. Distributions of the main physical quantities describing the molecular cloud lifecycle in 54 PHANGS galaxies. From left to right, we show a Gaussian kernel density estimate of the cloud lifetime (t_{CO}), the feedback time-scale (t_{fb}), the average separation length between independent star-forming regions (λ), and the integrated star formation efficiency (ϵ_{sf}). For each histogram, the mean (black dot) and 16-84 percentile range (error bar) are indicated at the top of the panel. Taken from Kim et al. (2022a).

The overall measured range of molecular cloud lifetimes and the feedback time-scales are consistent with that found in previous studies, those using cloud classification methods (e.g. Engargiola et al. 2003; Kawamura et al. 2009), and those using the same statistical method (Kruijssen et al. 2019; Chevance et al. 2020; Kim et al. 2021). This short feedback timescale implies that supernova explosions ($4-20$ Myr after star formation) take place in a medium that is already heavily pre-processed by early feedback.

For the 46 galaxies where we sufficiently resolve independent regions to get reliable measurements on λ, we find that λ ranges from 100 pc to 400 pc, with an average and standard deviation of 254 ± 79 pc. This is similar to the total cold gas disc thickness (100-300 pc; Heyer & Dame 2015; Patra 2020; Yim et al. 2020), as well as the range of values found in previous application of the same method to relatively nearby and well-resolved galaxies (100-250 pc; Kruijssen et al. 2019; Chevance et al. 2020; Kim et al. 2021). From the similarity of λ to the gas disc scale height, Kruijssen et al. (2019) have suggested that this characteristic length scale might be set when feedback-driven bubbles break out of the galactic disc and depressurise.

We measure a star formation efficiency per GMC of $0.7 - 7.5\%$ across our galaxy sample, illustrating that rapid stellar feedback strongly restricts the conversion of gas to stars in these clouds by limiting their lifetime. Our previous measurements of ϵ_{sf} (Kruijssen et al. 2019; Chevance et al. 2020; Kim et al. 2021) also fall within this range of values.

3. Relations with global galaxy and average cloud properties

In Figure 2, we show several statistically significant correlations identified between our measurements and galaxy properties. In brief, t_{CO} shows positive correlations with quantities related to galaxy mass (e.g. stellar mass $M_{*,global}$), as well as with the molecular gas surface density (Σ_{H_2}). These correlations could be caused by higher gas pressures at higher galaxy masses or higher gas surface densities, which may extend the cloud lifetime. Additionally, the higher pressures allow us to also detect the extended envelopes of the GMCs, unlike in low-surface density (atomic gas-dominated) environments where CO is only tracing the densest centres of the GMCs. Finally, in low-mass (low-metallicity) and less dense environments, the molecular gas may be CO-dark, as these environments require higher gas column density in order to shield CO molecules from being dissociated. All of these mechanisms would make the CO-bright GMC lifetime increase with galaxy mass or gas surface density.
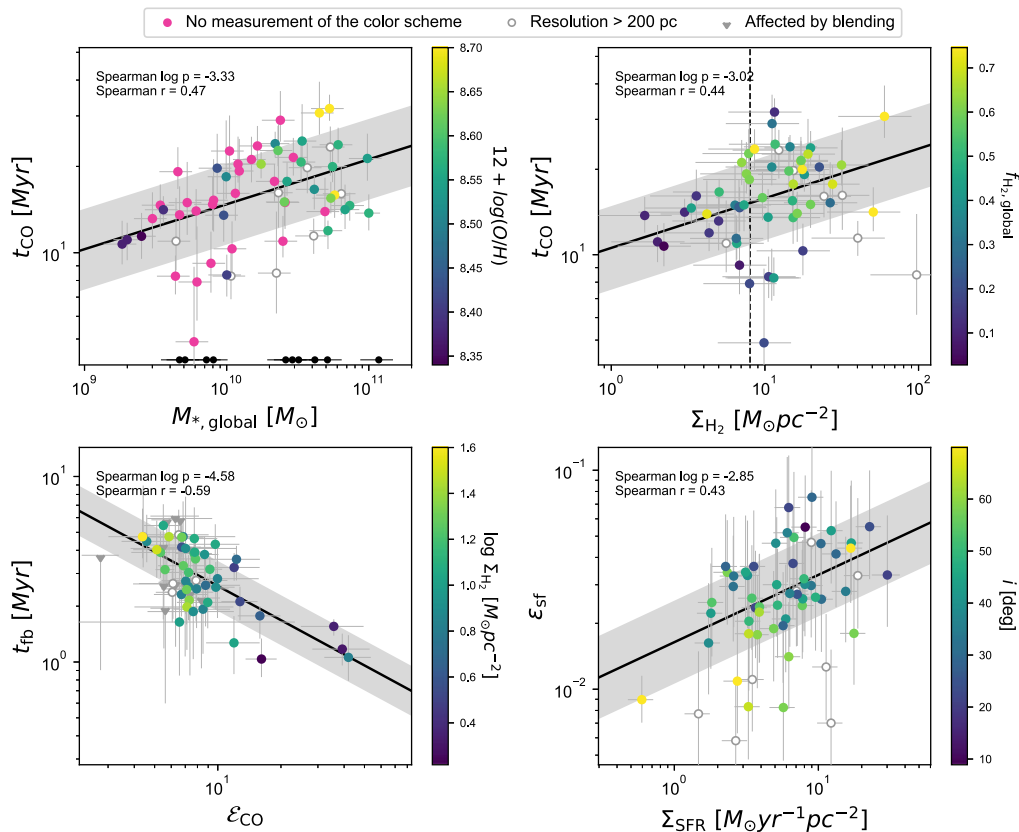
Figure 2. Examples of four statistically significant correlations between our measurements and galactic properties. In the upper panels, the measured cloud lifetime (t_{CO}) is shown as a function of galaxy stellar mass ($M_{*,global}$; left) and molecular gas surface density (Σ_{H_2}; right), with points colour-coded by metallicity ($12 + \log(O/H)$) and molecular gas fraction ($f_{H_2,global}$), respectively. The density proposed by Chevance et al. (2020) to divide between internal dynamics and galactic dynamics-driven GMC lifetimes is indicated by the dashed line at $8\,M_\odot pc^{-2}$. In the bottom left panel, the measured feedback time-scale (t_{fb}) is shown as a function of the surface density contrast between CO emission peaks and the galactic average (ε_{CO}), colour-coded by the molecular gas surface density (Σ_{H_2}). The bottom right panel shows the integrated star formation efficiency (ϵ_{sf}) as a function of SFR surface density (Σ_{SFR}), where the points are colour coded by galaxy inclination (i). Galaxies without measurements corresponding to each colour bar scheme are denoted in magenta. Gray circles are the galaxies with resolution worse than 200 pc. Gray triangles indicate upper limits for galaxies suffering from blending of sources (see Kim et al. 2022a). All gray points are excluded from the correlations. For individual data points, 1σ uncertainties are shown. In each panel, the best-fitting linear regression (solid line), 1σ scatter of the data around the fit (shaded area), and the Spearman p-values and correlation coefficients are indicated. Masses of the ten galaxies excluded from our sample due to insufficient emission peaks are also shown (black circles, top left panel). Taken from Kim et al. (2022a).

The feedback time-scale t_{fb} also shows correlations with quantities related to galaxy mass, most likely because t_{CO} and t_{fb} are correlated. In addition, t_{fb} also shows an interesting relation with ε_{CO}, which is the surface density contrast measured in a CO map between emission peaks and the galactic average. We find that t_{fb} is shorter with increasing ε_{CO} (i.e. towards sharper emission peaks). This can be physically understood as a direct consequence of stellar feedback, with CO emission becoming undetected faster after
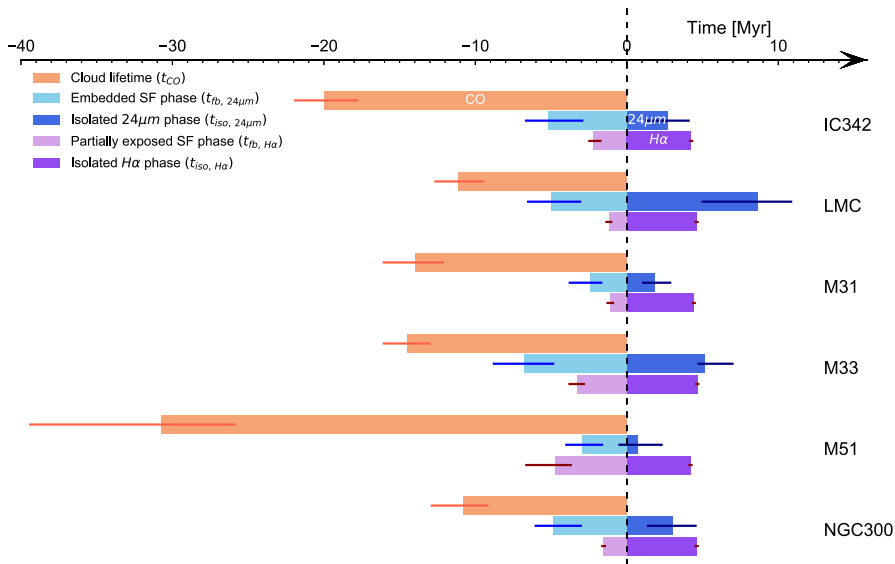
Figure 3. Timelines describing the evolution of molecular clouds from an inert gas phase, to an embedded star-forming phase, and then finally to exposed young stellar regions. The time during which CO is visible (t_{CO}) is indicated in orange, the time during which $24\,\mu m$ and Hα are visible without CO are shown respectively in dark blue and dark purple. The timescales associated to the feedback phase, during which both CO and SFR tracer emissions are observed co-spatially are shown in light blue (for $24\,\mu m$) and light purple (for Hα). The corresponding 1σ error bars are also indicated. We note that for M51 the feedback timescale constrained using $24\,\mu m$ ($t_{\rm fb,\,24\,\mu m}$) is likely to be biased by deconvolution artifacts (see Kim et al. 2021 for details). Taken from Kim et al. (2021).

the onset of massive star formation when the surrounding medium is sparser, facilitating a rapid dispersal of the gas.

The star formation efficiency $\epsilon_{\rm sf}$ shows a correlation with the SFR surface density. This can be at least partly understood by the fact that, naively, a higher SFR would naturally lead more stars formed within a cloud in a given time, and therefore to a higher integrated star formation efficiency per cloud. However, other factors can also contribute to this trend such as the tight correlation between $t_{\rm CO}$ and $\Sigma_{\rm H_2}$, as well as the dependence of extinction correction on inclination, as indicated by the data point colours in Figure 2 showing a trend between i and $\Sigma_{\rm SFR}$.

4. Duration of the early phase of massive star formation in five nearby galaxies

While Hα is typically used as a SFR tracer, the earliest phases of star formation are heavily embedded and invisible in Hα due to the extinction from the surrounding dense gas and dust. Therefore, the duration of these early phases of star formation and the time that clouds spend being truly inert are still poorly constrained, and so is the time needed for the feedback from these embedded stars to pierce through the natal cloud and enable the detection of Hα.

The $24\,\mu m$ emission in the mid-infrared observed by the Multiband Imaging Photometer aboard the Spitzer Space Telescope provides an unbiased tracer of embedded massive star formation (Kennicutt & Evans 2012). This mid-infrared emission originates from stochastically heated small dust grains that do not require ionizing photons to be excited but do empirically correlate with tracers of massive star formation and so can be

used as a tracer of the presence of large amounts of dust reprocessed photospheric light from massive stars.

In Kim et al. (2021), we apply the same statistical method (Kruijssen et al. 2018) to six nearby star-forming galaxies using CO, *Spitzer* 24 μm, and Hα emission maps, tracing molecular clouds, embedded star formation, and exposed star formation, respectively. The small size of this sample results from the limited resolution of the *Spitzer* 24 μm observations (6") and the requirement that the observations need to resolve each galaxy into its distinctive units of star formation (e.g. GMCs and HII regions, typically separated by ~ 100 pc). In Figure 3, we show an illustration of the evolutionary timelines of molecular clouds and star-forming regions in the six galaxies included in our analysis. GMCs initially emit only in CO, then in 24 μm after the onset of star formation and finally in Hα when the star-forming regions become (partially) exposed. This provides systematic constraints on the duration of the embedded phase of star formation for five of these six galaxies. For M 51, we were not able to derive a reliable result, because the deconvolution algorithms applied to the 24 μm map (Dumas et al. 2011) did not lead to a sufficient data quality to successfully perform this measurement. For the remaining five galaxies, we find that the embedded phase of massive star formation, defined as the time for which CO and 24 μm overlap ($t_{\text{fb}24\,\mu\text{m}}$), to last for 2−7 Myr, or 20−50% of the cloud lifetime. This indicates that clouds are devoid of massive stars for 50−80% of their lifetime. The first half of the embedded phase (1−4 Myr) is heavily obscured and invisible in Hα emission.

5. Conclusion

We have quantified the evolutionary lifecycle of GMC formation, evolution, and dispersal across 54 nearby disc galaxies, which is the largest and most statistically complete sample to date. We have demonstrated that this lifecycle depends on the large-scale galactic environment. We have identified strong correlations between GMC evolutionary time-scales and the host galaxy properties (e.g. stellar mass, molecular gas surface density), revealing the role of galactic-scale processes in the small-scale GMC lifecycle. In the 5 most nearby galaxies of our sample, we were able to refine this timeline further and constrain the heavily obscured phase using the *Spitzer* 24 μm observations. In the future, we plan to further extend and refine this evolutionary timeline, for a subset of our parent galaxy sample, by including other observations at different wavelengths: ionised emission lines from MUSE, mid-infrared from the *James Webb Space Telescope*, and HI from the VLA and Meerkat. This will allow us to determine the time-scales of all the successive phases of the gas that participates in star formation, identify their dependences on the large-scale environment, and derive constraints on the physical mechanisms that regulate GMC evolution and star formation in galaxies.

References

Chevance M., Kruijssen J. M. D., Hygate A. P. S., *et al.*, 2020, *MNRAS*, 493, 2872
Chevance M., Krumholz, Mark R. and McLeod, Anna F., *et al.*, 2022, arXiv:2203.09570

Dumas G., Schinnerer E., Tabatabaei F. S., *et al.*, 2011, *AJ*, 141, 41

Engargiola G., Plambeck R. L., Rosolowsky E., Blitz L., 2003, *ApJS*, 49, 343

Heyer M., Dame T. M., 2015, *ARAA*, 53, 583

Kawamura A., Mizuno1 Y., Minamidani T., *et al.*, 2009, *ApJS*, 184, 1

Kennicutt, R. C., & Evans, N. J. 2012, *ARAA*, 50, 531

Kim J., Chevance M., Kruijssen J. M. D., *et al.*, 2021, *MNRAS*, 504, 487

Kim J., Chevance M., Kruijssen J. M. D., *et al.*, 2022a, *MNRAS*, 516, 3006

Koda, J. and Scoville, N. and Sawada, T., *et al.*, 2009, *ApJL*, 700, 132

Kruijssen J. M. D., Longmore S. N., 2014, *MNRAS*, 439, 3239

Kruijssen J. M. D., Schruba A., Chevance M., *et al.*, 2019, *Nature*, 569, 519

Kruijssen J. M. D., Schruba A., Hygate A. P. S., *et al.*, 2018, *MNRAS*, 479, 1866

Krumholz M. R., 2014, *Phys. Rep.*, 539, 49

Leroy A. K., Schinnerer E., Hughes A., *et al.*, 2021, *ApJS*, 257, 43

Lu, A. and Boyce, H. and Haggard, D., *et al.*, 2022, *MNRAS*, 514, 5035

Patra N. N., 2020, *A&A*, 638, A66

Scannapieco, C. and Wadepuhl, M. and Parry, O. H., *et al.*, 2012, *MNRAS*, 423, 1726

Scoville N. Z., Hersh K., 1979, *ApJ*,229, 578

Sun J., Leroy A. K., Rosolowsky E., *et al.* 2022, *AJ*, 164, 43

Ward, J. L. and Kruijssen, J. M. D. and Chevance, M., *et al.* 2022, *MNRAS*, 516, 4025

Yim K., Wong T., Rand R. J., Schinnerer E., 2020, *MNRAS*, 494, 4558

Zabel, N. and Davis, T. A. and Sarzi, M., *et al.* 2020, *MNRAS*, 496, 2155